Marine Pollution Bulletin 223 (2026) 118996

Contents lists available at ScienceDirect

Marine Pollution Bulletin

journal homepage: www.elsevier.com/locate/marpolbul

Temporal trends of pollution in an estuary affected by phosphogypsum leachates and acid mine drainage: Waste management implications

M. del Caño-Mármol [a], A. Barba-Lobo [a,*], E.G. San Miguel [a], J.L. Guerrero [b], J.P. Bolívar [a]

[a] Radiation Physics and Environment Group (FRYMA), Department of Integrated Sciences, Center for Natural Resources, Health and Environment (RENSMA), University of Huelva, 21007, Huelva, Spain
[b] Global Earth Change and Environmental Geology Research Group, Department of Biology and Geology, Physics and Inorganic Chemistry, Universidad Rey Juan Carlos, c/Tulipán s/n, Móstoles, 28933, Spain

ARTICLE INFO

Keywords:
Estuary
Phosphogypsum
AMD
Heavy metals
Radionuclides
Pollution index

ABSTRACT

The Huelva estuary has been historically impacted by multiple pollution sources, including acid mine drainage (AMD), industrial emissions, and discharges from phosphogypsum (PG) piles. This study analyses the concentrations of heavy metals, major and trace elements, and radionuclides from the ^{238}U series in two sediment cores collected from the Tinto River estuary: one adjacent to the PG piles (Core 1) and the other on the opposite riverbank (Core 2). A reference core from the Piedras River was used to establish natural background levels. Core 1 provides a clear stratigraphic record of industrial activity, showing three contamination phases. The open-discharge period (60–30 cm) is characterized by extremely high values of P (~4 %), ^{238}U (~1200 Bq·kg^{-1}), ^{226}Ra (~800 Bq·kg^{-1}), and metals such as As (~4700 μg·g^{-1}) and Pb (~3000 μg·g^{-1}). Contamination indices (EF, Igeo, PERI) peak in this interval, confirming severe ecological risk. A decline from 30 to 10 cm reflects the shift to closed-circuit waste management, although U and P persist due to PG leaching. The surface layer (0–10 cm) records a marked reduction, but concentrations remain above background, evidencing long-term legacy pollution. The sedimentation rate (sr = 1.2 cm/yr) provides high temporal resolution. In contrast, Core 2 shows attenuated contamination restricted to the upper 20 cm, with lower radionuclide activities (^{226}Ra ~ 80 Bq·kg^{-1}, ^{210}Pb ~ 90 Bq·kg^{-1}) and metals, and a reduced sr = 0.4 cm/yr. Profiles suggest diffuse AMD influence rather than direct PG input. PCA differentiates contamination sources, confirming PG-dominated inputs in Core 1 and AMD-related contributions in Core 2.

1. Introduction

The Tinto and Odiel rivers, located in the southwestern Iberian Peninsula, constitute a fluvial system extensively studied due to its relevance and the substantial environmental impact it has undergone (Vidal-Garduño et al., 2025) These rivers drain a substantial portion of the Iberian Pyrite Belt (IPB), one of the largest and most mineralogically diverse massive polymetallic sulfide deposits that exist in the world (Sáez et al., 1999). The IPB spans approximately 250 km in length and 30–50 km in width, extending from southeastern Portugal to northeastern Huelva (Spain). The intensive historical mining activities developed from the second half of 19th century (Second Industrial Revolution) in this area has generated a deep environmental impact by AMD (van Geen et al., 1997; A. Valenzuela and Pascual, 2002; Pérez-López et al., 2025).

AMD results from the oxidation of sulfide minerals, especially pyrite (FeS_2), which, upon interacting with water and dissolved atmospheric oxygen, releases ferrous iron (Fe^{2+}) and causes intense acidification of the aquatic environment with pH values as low as 1 to 2 (Aduvire, 2006; Nieto et al., 2007). Additionally, minerals such as sphalerite (ZnS), galena (PbS), chalcopyrite ($CuFeS_2$), arsenopyrite (FeAsS), and pyrrhotite ($Fe_{1}S$) contribute to AMD formation and the mobilization of heavy metals within the aquatic system (Williams and Block, 2015; Gao et al., 2025).

Both rivers converge in the common estuarine system known as Huelva Estuary. When these waters (pH ~ 2–4) are mixed with the seawater (pH ~ 8.0) a co-precipitation of dissolved elements is produced (Papaslioti et al., 2024). Consequently, a large proportion of the toxic metals and metalloids transported to the estuary, either in dissolved form or as colloids, precipitate or coprecipitate with iron oxyhydroxides

* Corresponding author.
E-mail address: alejandro.barba@dci.uhu.es (A. Barba-Lobo).

https://doi.org/10.1016/j.marpolbul.2025.118996
Received 4 September 2025; Received in revised form 11 October 2025; Accepted 12 November 2025
Available online 21 November 2025

and other secondary minerals, leading to their immobilization in particulate form and eventual accumulation in the sediments (Casanueva Marenco, 2014; Liu et al., 2021). As result, these rivers annually contribute to the estuary approximately $7.9{\cdot}10^3$ t of Fe, $5.8{\cdot}10^3$ t of Al, $3.5{\cdot}10^3$ t of Zn, $1.7{\cdot}10^3$ t of Cu and $1.6{\cdot}10^3$ t of Mn, these values represent an important fraction of the global gross flux of dissolved metals (mainly Zn and Cd) transported by rivers into the ocean (Olías et al., 2006).

Industrial pollution has also had a significant and lasting impact on the Huelva Estuary, with a legacy closely tied to the establishment and evolution of the local chemical industry since the 1960s. Among the key milestones was the launch of a fertilizer production plant, which generated phosphoric acid by reacting to the phosphate rock (PR) with sulfuric acid. This industrial process gave rise to vast quantities of PG as a by-product, whose management has been a challenge over time, changing management policies and the impact that this waste has left on the environment.

The phosphate rock used in Huelva originated mainly from Morocco and contained ^{238}U series radionuclides at concentrations of around 1600 Bq·kg^{-1}—approximately 50 times higher than those found in unpolluted soils. During the acid attack process, a large fraction of these radionuclides remained within the PG: around 20 % of the U, more than 70 % of the Th, and over 95 % of Ra, Pb, and Po were retained in the waste. As a result, PG is classified as a Naturally Occurring Radioactive Material (NORM).

In addition to its radioactive content, PG also retains residual phosphoric acid within its pores, which contributes to its high acidity (pH ≈ 1.5) and enhances the mobility of hazardous elements like cadmium, arsenic, fluoride, and phosphate. Over the decades, the management of these residues has varied considerably, depending on industrial priorities, regulatory frameworks, and public environmental awareness.

1. **Initial Stage: open-cycle discharge policy (1965–1997):** Phosphoric acid production began in 1965 using sulfuric acid and fluorapatite phosphate rock as raw material, which is rich in uranium and its radioactive decay products. This process generated approximately 2.5 million tons of PG annually. Of this, 20 % was directly discharged into the Odiel River, while the remaining 80 % was stored in large settling ponds built on the Tinto River marshes, giving rise to what are now commonly known as "phosphogypsum piles/stacks". During this period, Zones 1 and 2 were created, as shown in Fig. 1. The fresh PG, mixed with seawater (20 % PG, 80 % seawater), was pumped into the ponds to settle. The resulting acidic water (pH ~1.5–2.0), containing high levels of pollutants, was discharged untreated into the Tinto estuary, around 10–15 millions of m^3 per year (Bolívar et al., 1995). Zone 1 was restored in 1990–92 period with a 40 cm of layer soil (Mas et al., 2006).

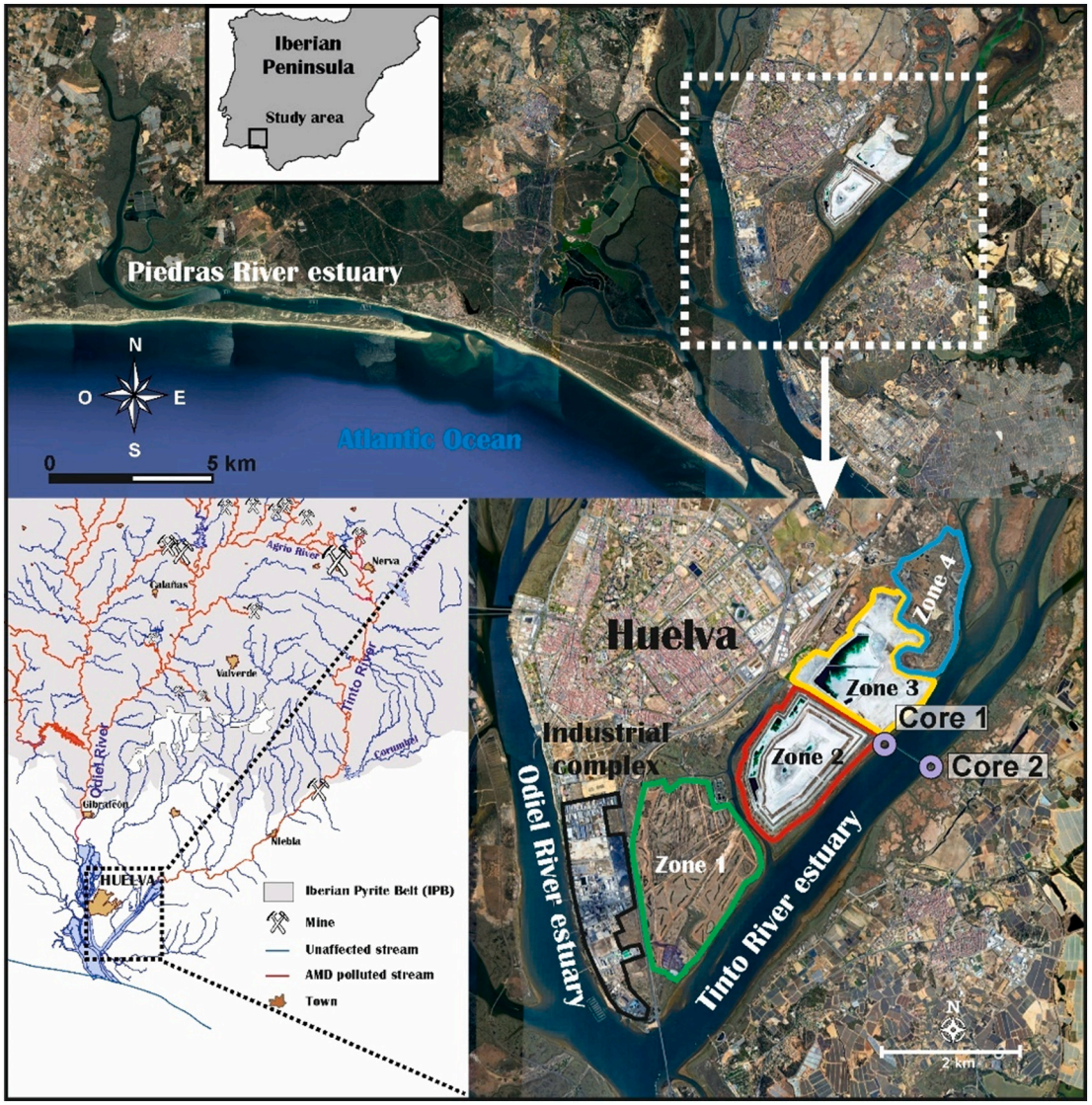

Fig. 1. Sampling location in the Huelva estuary, showing the positions of the sediment cores collected for this study.

2. **Closed waste management method (1998–2010):** A closed-loop freshwater system was introduced to transport PG to Zone 2, reducing liquid releases into the Huelva estuary by over 95 % (Mas et al., 2006). This shift in waste management was implemented in response to changes in environmental policy following the OSPAR Convention agreements, which aimed to eliminate discharges of hazardous substances into the marine environment. As a result, from 1998 until the end of production on December 31, 2010, Zone 2 became the main disposal site, forming a 20-meter-high pyramidal pile. However, despite the closed-circuit design, many points along the pile still exhibited lateral outflows discharging into the Huelva estuary.
3. **Current Situation:** Nevertheless, from 2011 until now many acidic outflows from the PG piles have been identified producing an estimated annual release into the estuary of about 10^5 m^3 (Pérez-López et al., 2016). Zone 2 has a height about 20 m and Zone 3 has a height of 5 m of PG, and zone 4 was restored in 2000–05 with more than 1 m of soils mixed with inert construction wastes (Macías et al., 2017). Zones 2 and 3 are nowadays unrestored, but in September 2024 started their remediation. The project involves sealing all points of acid leachate leakage across the four zones with impermeable barriers. Zones 2 and 3 are being restored by using a 2 mm thick geomembrane, a 60 cm layer of compacted clay, a drainage layer of approximately 30 cm, and finally a 50 cm thick layer of vegetated soil (*Restore 20/30 – Proyecto de clausura de las balsas de fosfoyeso*. (s. f.), 2025)

Both sources, direct discharges (up to 1997) and leachates from PG stacks, have left distinct geochemical signatures in the Huelva estuary (Pérez-López et al., 2010). The former responsible for a marked "radiological footprint" and the latter continuing to contribute to pollution. Furthermore, AMD upstream mining operations also introduces a characteristic geochemical and radiological fingerprint, resulting from the oxidation of sulfide. Therefore, this study uses the specific composition of both PG residues and AMD-affected waters and sediment to identify and distinguish the main sources of contamination present in the system.

In particular, elements such as P, repeatedly identified as an excellent tracer of the impact of PG stacks and the fertilizer industry due to its high mobility in acidic pore water (Guerrero et al., 2019); U, associated with the acidic liquid fraction (Bolívar et al., 2009), also highly mobile and strongly correlated with P; and radionuclides of the ^{238}U series (^{226}Ra, ^{210}Pb, ^{230}Th), which, although they remain predominantly in the solid matrix of PG (>95 %) and are strongly bound to gypsum (Bolívar et al., 2009), can still be released under specific environmental conditions, such as acidic pH, redox changes, increased ionic strength, or the presence of complexing agents, serve as reliable geochemical markers of PG influence, particularly through leachates (Barba-Lobo et al., 2024). Several trace metals exhibit concentrations orders of magnitude above background levels and show strong correlations with P, further supporting their role as indicators of PG leachate input. While ^{226}Ra is virtually absent from liquid fractions rich in P_2O_5, both ^{230}Th and ^{210}Pb are detectable (Bolívar et al., 2009), with their affinity for phosphoric acid following the order: U-isotopes > ^{230}Th > ^{210}Pb > ^{226}Ra. In sediments, ^{226}Ra and ^{210}Pb display a behavior similar to P, although they are less mobile.

Conversely, Fe, a well-established tracer of AMD (Guerrero et al., 2019), together with As and Zn are typical indicators of this source, originating from the oxidation of sulfide-rich minerals during the acid drainage process (Olías et al., 2006).

Throughout this study, these geochemical and radiological markers will be used to reconstruct the temporal evolution of pollution, to distinguish overlapping contamination events through their specific fingerprints, and to evaluate the effectiveness of the various waste management strategies applied in the estuary over time.

This study aims to address the environmental challenges affecting the Huelva Estuary by providing a comprehensive and up-to-date assessment of its pollution status. To achieve this, two sediment cores were analyzed one taken near PG piles and the other from the opposite riverbank. The objectives are to reconstruct temporal trends in contamination, identify major pollution events, and determine their potential sources.

Beyond the local context, the sedimentary record from the Huelva Estuary offers valuable insights into the long-term environmental impact of industrial activities and AMD. As such, this study may provide useful reference data for understanding the time evolution of pollution in other estuarine or coastal systems affected by similar contamination sources.

2. Materials and methods

2.1. Sampling

In November 2021, two sediment cores from the Tinto River estuary and one from the Piedras River (reference area) were collected. The Piedras River was used as reference to establish the background levels for the Huelva estuary, since it shares similar geochemical properties that Huelva estuary but without any influence from AMD, PG deposits, or nearby industrial activities (see Fig. 1). The measurements for the reference background used by Barba-Lobo et al. (2024) have been completed, measuring the entire core rather than one out of every three samples. Each core, measuring about 60 cm in depth, was sectioned into 2 cm-thick slices (Fig. A.1, Supplementary Material). The samples were subsequently dried at 60 °C until reaching a constant weight, then grounded and homogenized using an agate mortar. Major, minor, trace elements and radionuclides were determined in different sections of the sediment cores.

2.2. Characterization technique

The concentrations of major, minor, and trace elements were determined using inductively coupled plasma mass spectrometry (ICP-MS) and optical emission spectrometry (ICP-OES) at Activation Laboratories (Actlabs, Ontario, Canada), following a digestion process with strong acids, including hydrofluoric acid, and a subsequent mixture of nitric and perchloric acids. Granulometric analysis was performed using laser diffraction with a Malvern Mastersizer 2000 at the General Services of the University of Huelva, where the organic matter and calcium carbonates were removed in order to do the granulometry analysis using laser diffraction. Radionuclides were determined exclusively by alpha spectrometry, applying a specialized radiochemical method developed by the laboratories at the University of Huelva (Barba-Lobo et al., 2022).

2.3. Quality control

Quality control of ICP and ICP-OES measurements was ensured through the inclusion of one blank every five samples, one certified reference material every ten samples, and one replicate sample.

To ensure the reliability of the results obtained by the different analytical techniques, several quality checks were performed, including comparisons with certified reference materials and intercomparison exercises promoted by IAEA and CSN (Spanish Nuclear Safety Council), such as between ICP-based and spectrometric techniques.

To validate the alpha spectrometry results, ^{238}U activity was compared to values estimated from uranium concentrations measured by ICP, using the IAEA conversion factor for natural uranium (12.33 mBq/g of ^{238}U per μg/g of natural U). The good agreement between both methods confirms the consistency and accuracy of the data.

2.4. Pollution indexes

2.4.1. Enrichment factor

The enrichment factor (EF) is a widely used tool for evaluating anthropogenic pollution in soils and sediments by comparing the concentration of a target element to that in a reference material, normalized using a conservative element to account for natural background variability. Aluminum is commonly selected as the normalizer due to its chemical stability and low tendency to become enriched in estuarine environments, thus minimizing the effects of natural geochemical processes. The EF is calculated as:

$$EF = \frac{\left(\frac{C_i}{C_{Al}}\right)_s}{\left(\frac{C_i}{C_{Al}}\right)_r}$$

where C_i is the concentration of the element "*i*" in the sample "*s*" and reference "*r*" (Piedras river core), and C_{Al} is the corresponding concentration of aluminum. The enrichment factor is categorized into seven levels to assess the extent of anthropogenic influence on a given element. The degree of enrichment is categorized according to the following ranges: <1 (not enrichment), 1–3 (minor), 3–5 (moderate), 5–10 (moderately severe), 10–25 (severe), 25–50 (very severe), and >50 (extreme) (Chen et al., 2007). This classification system provides a standardized way to interpret and compare contamination levels across different studies and environments.

2.4.2. Contamination degree based on the EF (CD_{EF})

To simplify the interpretation of enrichment across multiple elements and avoid redundancy, individual Enrichment Factors were moved to supplementary material. Instead, a Contamination Degree based on the EF (CD_{EF}) for the whole sample is calculated as the arithmetic mean of the EF values for all analyzed elements, specially toxic heavy metals:

$$CD_{EF} = \frac{\sum_i^n EF_i}{n}$$

where n is the number of elements and EF_i represents the enrichment factor of each element.

By averaging the normalized EFs, the CD_{EF} provides a comprehensive overview of the general enrichment status of the samples. This approach not only highlights global trends but also facilitates comparisons between different sampling points or zones. The CD_{EF} serves as a useful metric to summarize the anthropogenic impact on the sediment matrix, offering a holistic perspective of contamination levels while maintaining methodological rigor.

2.4.3. Geoacumulation index

The geoaccumulation index (I_{geo}), developed by (Müller, 1979) is a widely applied tool for assessing the accumulation of elements in sediments and distinguishing between natural and anthropogenic contributions. It is calculated using the equation:

$$Igeo = log_2\left(\frac{C_i}{1.5C_r}\right)$$

where C_i represents the concentration of element "i" in the sediment, and C_r is the corresponding geochemical background value. Factor 1.5 accounts for natural variability in the element's concentration, minimizing the impact of minor anthropogenic influences. This correction factor ensures more reliable differentiation between natural and human-induced contamination.

The I_{geo} is categorized into seven classes (Qingjie et al., 2008): ≤0 (practically uncontaminated), 0–1 (uncontaminated to moderate contamination), 1–2 (moderate contamination), 2–3 (moderate to strong contamination), 3–4 (strong contamination), 4–5 (strong to very strong contamination, >5 (very strong contamination).

2.4.4. Potential Ecological Risk (PER) and potential toxicity of a sample (PT)

Potential Ecological Risk (PER) is a tool used to evaluate the toxicity associated with the presence of heavy metals in the environment, considering both their concentrations and toxic potential. Originally introduced by (Hakanson, 1980), this method remains widely utilized with updates to toxicity coefficients in line with recent studies (Tripathi and Nema, 2025). Metals typically considered include Cd, Cr, Cu, Ni, Pb, Zn, and the metalloid As, due to their significant environmental impacts.

The PER for an element "i" is calculated using the definition find in Barba-Lobo et al. (2024):

$$PER_i = CF_i \cdot T_i$$

where CF is the contamination factor define as $CF_i = \frac{(C_i)_s}{(C_i)_r}$, which compares the metal concentration in the sample to a reference or background value, and T_i is the toxicity coefficient, reflecting the relative ecological risk of each metal based on its toxicity and natural abundance. For instance, updated toxicity coefficients (T_i) were determined as follows Cd = 30, As = 10, Cr = 2, Cu = 5, Ni = 5, Pb = 5, and Zn = 1, emphasizing their varied toxicological significance (Chen et al., 2020).

To assess the global potential risk of a sample, the Potential Toxicity index (PT) is computed by summing the PER values for all analyzed elements:

$$PT = \sum PER_i$$

The ecological risk is classified into categories: low (<40), moderate (40–80), considerable (80–160), and very high (>320) (Kerolli–Mustafa et al., 2015). This classification helps prioritize remediation efforts by identifying areas with higher environmental risks. This framework has proven essential for managing contaminated sites and implementing mitigation strategies effectively.

2.5. Statistical analysis

Principal Component Analysis (PCA) was conducted to facilitate data interpretation using XLSTAT software. The analysis began with the computation of the correlation matrix based on the original dataset. Subsequently, the factor matrix was derived using Spearman's correlation coefficients, as most of the elements did not follow a normal distribution. This step inherently standardizes each variable, ensuring that the analysis is not biased by differences in data magnitude or measurement scales (DelValls et al., 1998; Emmerson et al., 1997). The eigenvalues and scree plot were used to determine the number of principal components to retain. Variable loadings were analyzed to interpret the contribution of each parameter to the principal components, while observation scores were examined to evaluate sample clustering and potential spatial trends.

3. Results and discussion

Throughout this study, two cores corresponding to the Tinto estuary have been studied. For that, a reference baseline has been established using the estuary of the Piedras River due to its geographic proximity and its comparable chemical composition to the study area, representing typical concentrations found in uncontaminated sediments of this geographical area, with minor variations due to the natural presence of polymetallic sulfides associated with the IPB. These values are shown in the Table 1. Cu and Zn concentrations are considerably higher than those typically found in uncontaminated sediments (approximately 2–3 times greater). This enrichment is not due to direct impact from AMD, but rather to the river crossing a section of the IPB which results in a

Table 1
Background reference values used in this study, obtained from a core collected in the Piedras River during a sampling campaign conducted by the FRYMA (Física de las Radiaciones y Medio Ambiente) research team.

%	Al	Ca	Fe	Ti	K	Mg	P	S
	5.2	0.30	2.8	0.58	1.47	0.54	0.028	0.73

mg/kg	As	Cd	Cr	Cu	Ni	Pb	Zn	Y
	30	0.29	57	123	24	46	271	14

Bq/kg	^{238}U	^{230}Th	^{226}Ra	^{210}Pb	^{232}Th
	28	27	26	29	30

moderate geochemical input from naturally mineralized rocks.

A preliminary granulometric analysis was performed to confirm that all sediment cores share similar textural characteristics, typical of estuarine environments (Hossain et al., 2014). This step is essential, as sediment grain size significantly influences pollutant concentrations; fine-grained sediments have a higher specific surface area, which enhances the adsorption of heavy metals and radionuclides. This consistency in grain size distribution rules out any significant granulometric influence on the elemental concentration profiles, supporting the validity of the geochemical comparisons. Granulometric data are provided in the supplementary material (Tables A.1 and A.5), with a summary included in the Materials and methods section.

3.1. Major elements

To ensure a consistent comparison between the two sediment cores, the same set of major elements was determined in both: Fe, Al, S, K, P, Mg, Na, Ca, and Ti. Elements with concentrations exceeding 0.1 % were classified as major elements. Fig. 2 displays the vertical profiles of Fe, Al, S, K, and P for both cores, while the profiles of Mg, Na, Ca, and Ti are provided in Tables A.2 and A.6 of the supplementary material. Details regarding the analytical procedures and rationale for element selection are described in the Materials and methods section.

The elements as K and Al exhibit concentrations typical of uncontaminated sediments by comparing them with the values included in Table 1. This interpretation is further supported by comparison with the average concentrations reported by Rudnick and Gao (2003) for upper soils, reflecting their natural origin. Moreover, the similar vertical distribution of these elements in both sediment cores suggests that their presence is primarily controlled by natural geochemical processes, with negligible influence from anthropogenic activities.

In contrast, Core 1 shows significantly higher concentrations of elements such as Fe, S, Ca, and particularly P, with values exceeding those typically found in uncontaminated sediments. Fe concentrations in Core 1 range from 4.5 to 16.5 %, with an average value of 10.5 %. These values exceed the regional background levels for estuaries (1–5 %) as reported in previous studies (Delgado et al., 2012; Sousa et al., 2019). In comparison, Core 2 exhibits even higher average Fe concentrations, reaching 16 %, highlighting a markedly different pattern between the two cores. This significant increase suggests a strong contribution from AMD in core 2, which has been identified as the primary source of Fe in these sediments according to previous studies (Sainz et al., 2004). Additionally, surface sediment sampling conducted in the estuary reported Fe distributions ranging between 11 % and 23 %, consistent with the findings of this study (Borrego et al., 2002), demonstrating these results a clear pollution of Tinto estuary in relation to the background (Piedras estuary).

P exhibits markedly different behaviors in both cores, specifically, P is a key marker associated to the phosphoric acid production industry, helps to identify industrial contributions to these sediments since the AMD is not enriched in P (El Afifi et al., 2009; Guerrero et al., 2019) reflecting the influence of proximity to PG. In this estuarine environment, P is primarily transported as phosphate (PO_4^{3-}) in dissolved form, due to its high solubility under the extremely acidic conditions (pH ≈ 1–2) characteristic of PG leachates (Pérez-López et al., 2010). This behavior supports its use as a conservative tracer of PG-related pollution, particularly for distinguishing leachate inputs from AMD.

In Core 1, collected adjacent to the PG stacks, P concentrations are markedly elevated throughout the sediment profile, with values ranging from 0.91 % to 4.01 % and an average of 2.45 %. These values are two orders of magnitude higher than the regional geochemical background of 0.05 % (Rudnick and Gao, 2003; Barba-Lobo et al., 2024), confirming a strong input influence.

From the surface down to 24 cm depth, P concentrations remain relatively stable, ranging between 0.55 % and 1.55 %. Below this depth, from 24 to 60 cm, concentrations progressively increase, reaching up to 4.24 %. This shift likely reflects the change in industrial practices following the implementation of the closed-cycle PG management system in 1998, after which direct discharges into the estuary ceased and residues were confined within the stacks.

Assuming that the first 24 cm depth corresponds to the year 1998 and considering that the core was collected in 2021, an average sedimentation rate (*sr*) of approximately 1.04 cm/year can be estimated. The presence of elevated P concentrations down to the base of the core (58–60 cm) suggests that the entire sediment sequence was deposited during the period of industrial activity, which began in 1965, thus preserving a complete contamination record.

In Core 2, extracted from the opposite riverbank and located farther from the PG stacks, P concentrations in the deeper layers (60–22 cm) remain low and stable, ranging from 0.05 % to 0.18 %, with an average value of 0.11 %. These values are close to the natural geochemical background, suggesting that this section was deposited before the onset of industrial activity and is primarily influenced by AMD.

A noticeable increase in P concentrations begins at approximately 22 cm depth. From this point upward (22–0 cm), *P* values rise progressively, reaching a maximum of 1.5 % between 10 and 20 cm depth, with an average of 0.38 % in the upper section (0–22 cm). This enrichment is attributed to the impact of the phosphate industry, which began operations in 1965.

Assuming the contamination signal starts at 22 cm and the core was collected in 2021, the estimated *sr* is approximately 0.40 cm/year—significantly lower than that calculated for Core 1. This reduced rate is consistent with the core's distal location within the estuarine system.

In contrast to Core 1, the behavior of S in Core 2 does not indicate significant industrial input. S concentrations remain below 1 % throughout most of the profile and show a strong correlation with Al and K, as can be seen in the profiles of both elements, elements typically associated with natural aluminosilicate inputs (Rudnick and Gao, 2003), suggesting that S in this core is primarily of natural origin. A slight increase in S from 20 cm depth upward mirrors the trend observed for P and further supports the interpretation of industrial influence in the uppermost layers.

3.2. Trace elements

Trace elements (As, Y, Cd, Pb, Cr, Ni, Cu, and Zn) exhibit heterogeneous distribution patterns in both sediment cores, exceeding background reference values (Table 1) in most cases. The vertical profile of these elements is illustrated in Fig. 3.

Core 1 shows a particularly pronounced enrichment in deeper layers for elements such as As, Cd, and Pb, reaching concentrations up to about 60, 40, and 40 times higher, respectively, than background levels, and even doubling the values observed in Core 2. The vertical profiles of concentration of these elements reveal that most of them display

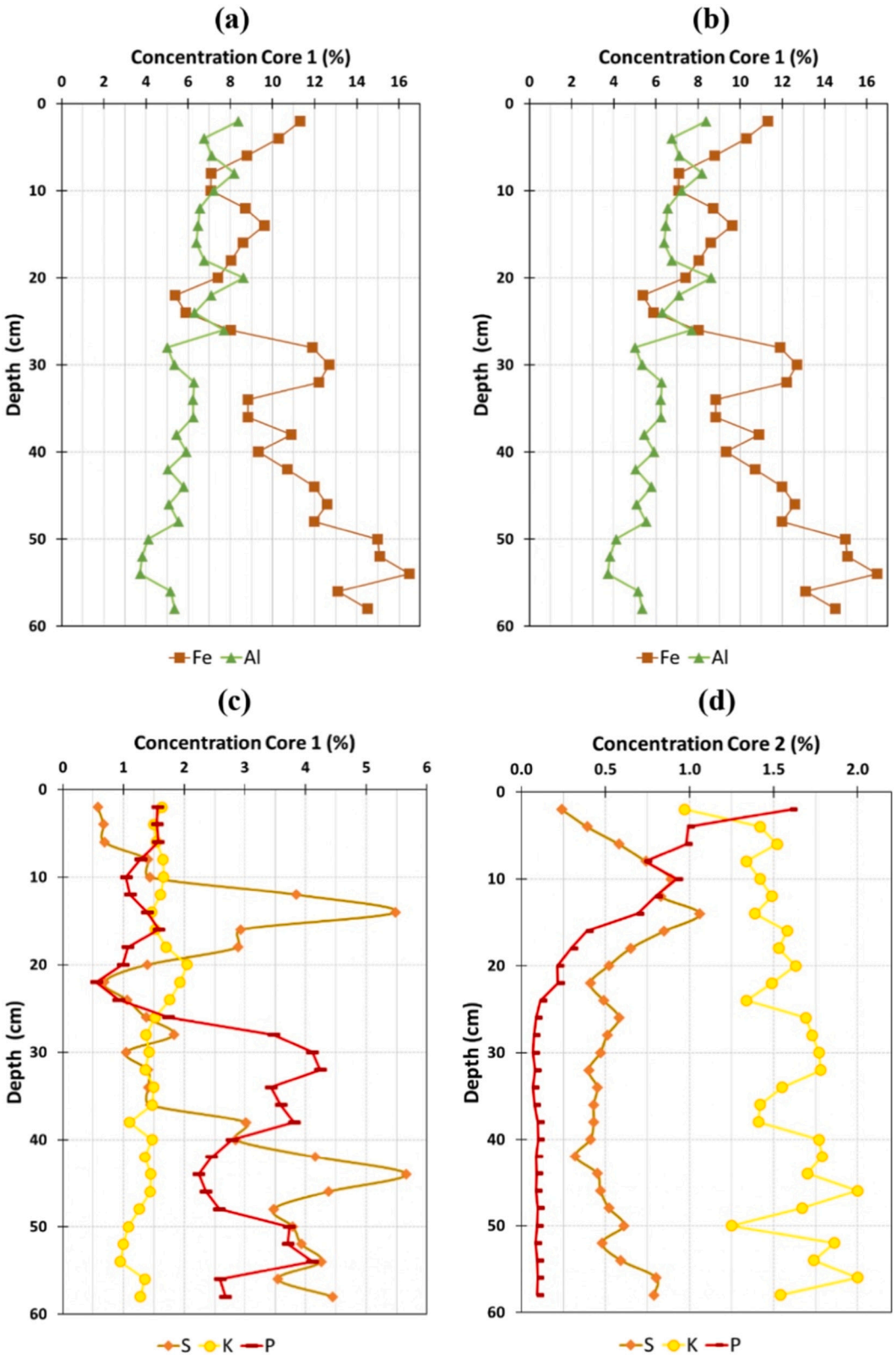

Fig. 2. Concentration of major elements for both cores, core 1 (left side) and core 2 (right side).

significant inflection points at specific depths, such as around 30 cm for As and Pb, and 20 cm for Cr and Y. These inflections are used as an indicative of the change in wastes policy, already discussed in the previous section. This pattern aligns with the previously described distribution of P, which serves as a marker for PG-related inputs. Notably, the co-occurrence of high P with peaks in Y, Cd, Cr and As supports their common origin in PG residues.

In contrast, Cu, Zn and Ni show relatively uniform behavior throughout the core 1, without the sharp peaks or declines observed in other elements, which could indicate a constant input over time or

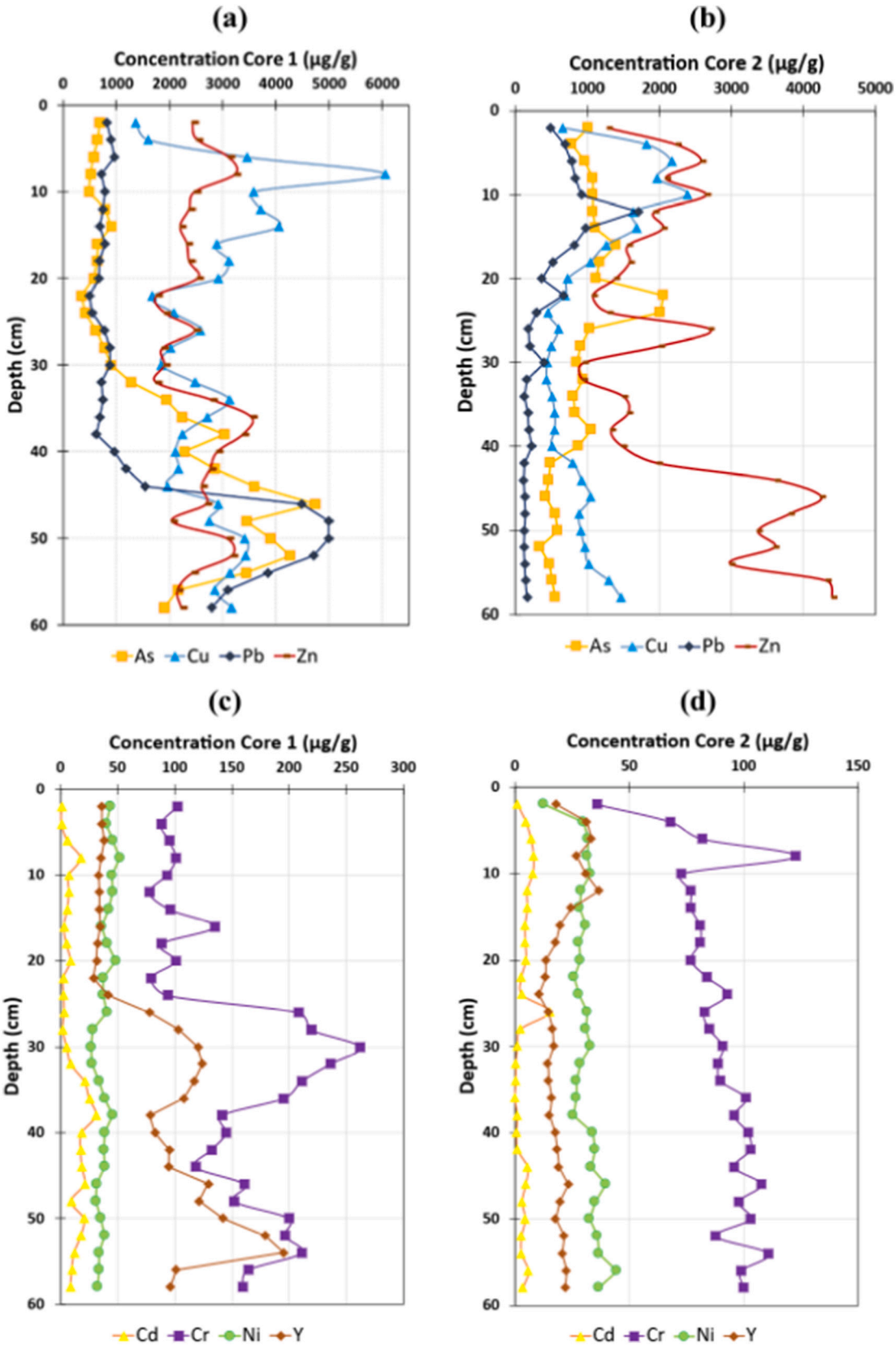

Fig. 3. Concentration of trace element for both cores, Core 1 (left side) and Core 2 (right side).

greater post-depositional mobility. Although Cd presents lower absolute concentrations compared to other elements, its ratio to the regional background is two orders of magnitude higher, and three orders of magnitude higher when compared to the average upper continental crust background (Rudnick and Gao, 2003).

In Core 2, the most enriched element relative to background levels is As, reaching concentrations up to 30 times higher around 24 cm. However, this represents only half the maximum value recorded in core 1, indicating a lower degree of contamination in this area. Zn, and to a lesser extent Cu, display similar vertical distributions and concentrations to those observed in core 1, suggesting a common and likely diffuse source, potentially linked to acid mine drainage, which exerts a more homogeneous influence across the estuarine system. In contrast, Y concentrations are up to five times lower than those in core 1, which may reflect both a reduced impact from the PG stacks and elemental composition between the two sampling sites. Overall, the trace element

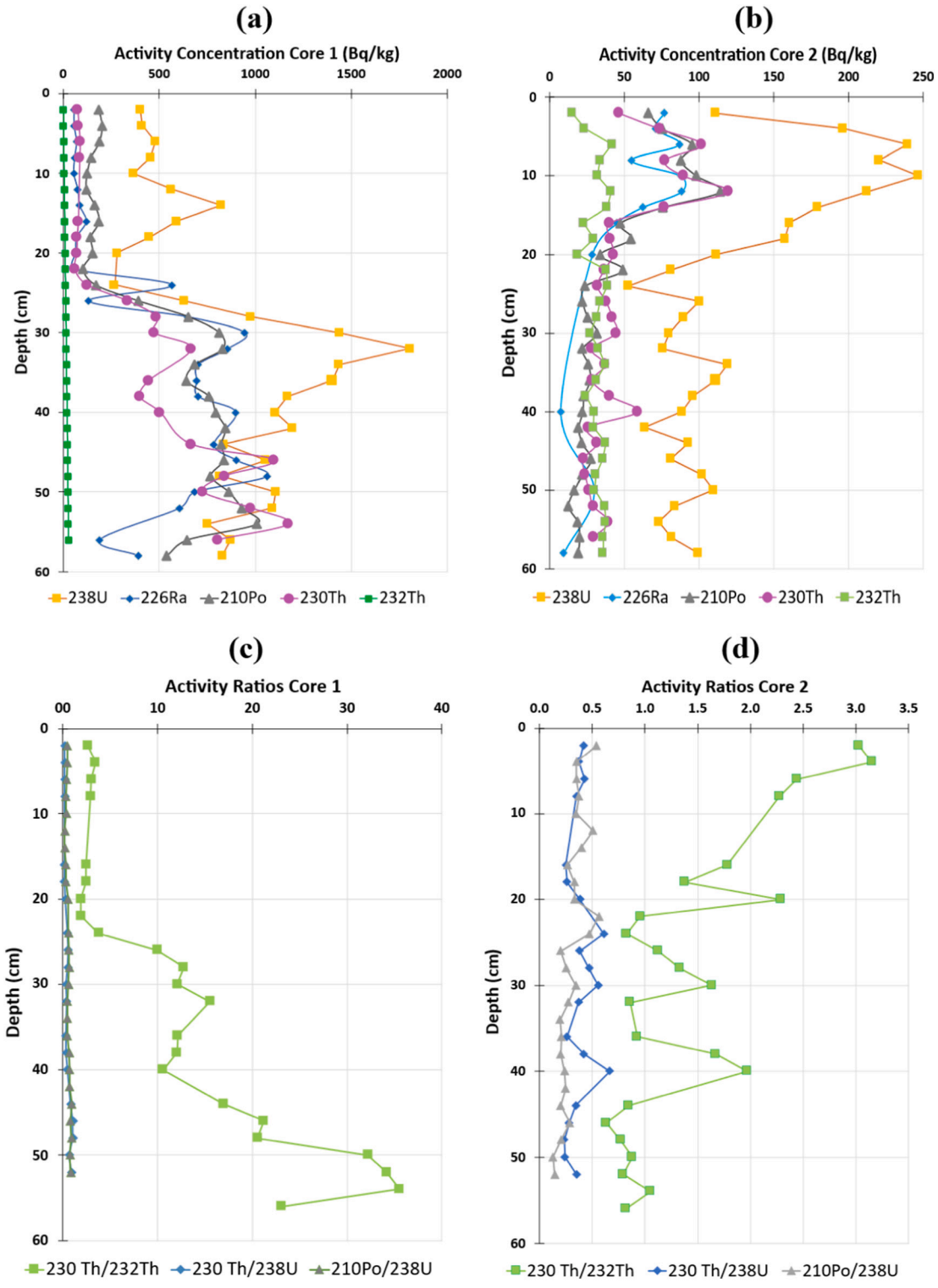

Fig. 4. Concentrations of radionuclides from the ^{238}U-series in cores 1 and 2 and activity ratios.

profiles suggest that their accumulation has been primarily controlled by proximity to contaminant sources and by post-depositional processes regulating element mobility and retention within the sediment matrix. In this core, metal concentrations tend to be higher in surface layers, although no clear enrichment pattern linked to historical waste management phases is observed. This may be due to the greater distance from direct discharge points and to the lower mobility of certain metals under the prevailing geochemical conditions. This will be analyzed in more detail in the contamination indices section.

Sediment Quality Guidelines (SQGs) have been developed in recent decades to evaluate and manage sediment contamination, evolving from purely chemical assessments to incorporate ecotoxicological criteria. Among the most widely applied benchmarks are the Effects Range Low (ERL) and Effects Range Median (ERM) values proposed by NOAA, which define threshold concentrations for toxic elements such as As, Pb, Cd, Cr, Cu, and Zn (see Table A.4 in supplementary material). ERL values represent levels below which adverse ecological effects are unlikely, whereas ERM values indicate concentrations above which such effects are more probable. These benchmarks, adapted for sediments and supported by extensive datasets, provide a robust framework for assessing ecological risk in aquatic environments under site-specific conditions.

Attending to these criteria, the comparison of measured concentrations in both sediment cores against NOAA's ERL and ERM guidelines reveals widespread contamination and substantial ecological risk, particularly in core 1. Most elements, especially As, Cd, Cu, Pb, and Zn, consistently exceed the ERM thresholds, indicating a high probability of adverse biological effects. In core 1, contamination is more intense and persistent, with As and Pb reaching extreme concentrations at mid-depths, while Cd also exceeds critical thresholds in a significant proportion of samples. Zn and Cu show a less stratified pattern but remain consistently elevated throughout, reinforcing their relevance as priority pollutants. In contrast, Cr and Ni remain closer to or within the ERL–ERM range, suggesting a comparatively moderate risk.

In core 2, although the enrichment is slightly less pronounced, the concentrations of As, Cd, Cu, Pb, and Zn still frequently surpass ERM values, reflecting a continued potential for ecological harm. Particularly notable is Cu, which exhibits intense and persistent contamination, with concentrations nearly an order of magnitude above the ERM limit in the central portion of the core. Pb and Zn also display critical exceedances, especially in surface layers, underscoring their mobility and long-term environmental persistence. Altogether, the ERL–ERM assessment confirms the high vulnerability of the estuarine system to heavy metal pollution and highlights the need for continued monitoring and potential remediation strategies in the most impacted zones.

3.3. Radionuclides concentrations and activity ratios

The activity concentrations of natural radionuclides in Core 1 exhibit well-defined vertical profiles (see Fig. 4) that reinforce the patterns previously discussed. A significant enrichment in ^{238}U series radionuclides is observed, particularly in the deeper layers (20–60 cm), corresponding to the period of open-cycle PG discharges (1965–1998). ^{238}U reaches activity concentrations of up to 1800 Bq/kg, greatly exceeding both the regional background level (~40 Bq/kg; Bolívar et al., 2009) and the value measured in the uncontaminated reference core (~28 Bq/kg). The ^{238}U profile is similar to the P one, with both peaking at approximately 30–40 cm depth, confirming the strong correlation between these two elements (see Fig. A.5, Supplementary Material) and supporting a common origin associated with PG leachates. This pattern is consistent with the high solubility and mobility of uranium in acidic environments (El Afifi et al., 2009).

In contrast, ^{226}Ra, ^{230}Th, and ^{210}Po are particle-reactive radionuclides, showing limited mobility in aqueous environments and a strong affinity for particulate matter (Bolívar et al., 1995). Their activity concentrations ranged from 60 to 1000 Bq/kg and exhibit sharp transitions at 22 cm depth. Above this depth, values decline and approach background levels (25–50 Bq/kg; UNSCEAR), consistent with the implementation of a closed-loop management system after 1998, when direct PG discharges ceased. This behavior can be corroborated by the calcium profile (see Fig. A.4) since PG is dehydrated calcium sulphate, which is directly associated with direct PG discharges. The decrease indicates that post-1998 contamination is mostly due to leaching, and not to direct input of PG solids, which are richer in ^{226}Ra and ^{230}Th.

Below 22 cm, the increase in ^{226}Ra and ^{230}Th corresponds to a period when PG was discharged as suspended fine material, due to the absence of water recirculation in the pumping system. This interpretation is also supported by the high ^{230}Th/^{232}Th activity ratios in this interval (reaching values up to 35), indicative of uranium-series disequilibrium and recent anthropogenic input. This parameter can be used to verify the stability of radionuclides in the system, determine potential recent inputs of uranium-enriched materials or their descendants and date sediment layers, particularly in those levels where equilibrium between radionuclides of the same series is disrupted. Attending to Fig. 4 the evolution of the ^{230}Th/^{232}Th activity ratio in Core 1 reveals three distinct periods of contamination. This ratio decreases progressively above 22 cm, stabilizing near 1 in the uppermost layers, in agreement with the natural isotopic equilibrium expected in the absence of recent contamination.

In Core 2, ^{238}U is the radionuclide with the highest concentrations, reaching values close to 250 Bq/kg. A rising trend towards the surface is observed, with remarkable peaks at depths of 10 and 6 cm, indicating anthropogenic enrichment in the upper layers. Nevertheless, as established earlier, the lower *sr* at this site means that the top 20 cm of sediment integrate the cumulative impact of industrial activity over several decades. As a result, the apparent surface enrichment does not necessarily reflect recent contamination events, but rather the long-term deposition of PG-derived pollutants under slower sediment accumulation conditions. This trend mirrors that of P, with both elements showing elevated concentrations around 20 cm depth, reinforcing their common origin.

The enrichment of ^{238}U in the upper layers is also accompanied by increases in other members of its decay chain, ^{230}Th, ^{226}Ra, and ^{210}Po (Fig. 4), as expected in systems affected by uranium-derived contamination (Hierro et al., 2013). However, the concentrations of these daughter radionuclides remain significantly lower than those observed in Core 1, and their vertical distributions are smoother, without abrupt transitions. This suggests that contamination in Core 2 has occurred primarily through dissolved-phase inputs (Wang and Wang, 2016), consistent with a more distant location from the PG stacks and the absence of direct deposition of particulate PG material.

^{226}Ra and ^{210}Po display moderate activity values, ranging from 50 to 100 Bq/kg in the upper 20 cm, slightly exceeding natural background levels (25–50 Bq/kg; UNSCEAR). For depths under 20 cm, 226Ra concentrations were similar to background values.

Finally, the concentrations of ^{232}Th remain low and uniform throughout both sediment column, with values comparable to those of uncontaminated soils typically between 25 and 50 Bq/kg. Moreover, when comparing the data between both cores (Core 1 and Core 2), no significant differences are observed, confirming that this element has not been enriched in the sediments affected by PG neither by AMD.

The ^{230}Th/^{232}Th activity ratio in Core 2 displays a noticeably irregular and variable profile, likely reflecting the low absolute activities and the close proximity of measured values. Despite this variability, a gradual upward trend can be observed above 20 cm depth. This increase aligns with the most affected sedimentary interval by industrial discharges, according to the accumulation pattern of this core. The observed rise in the ratio reinforces the interpretation that the upper 20 cm reflect the cumulative impact of anthropogenic inputs, although the overall signal remains much weaker compared to the more heavily contaminated Core 1.

3.4. Contamination indices

The contamination indices analyzed in this study focus on most relevant elements associated with decades of industrial activity, particularly P, trace elements, and alpha-emitting radionuclides. Data for other elements are provided in the supplementary material (Fig. A.6, Supplementary Material).

Overall, the trends observed in both sediment cores are consistent with studied in previous sections, as it can be observed in Fig. 5. In Core 1, EFs are lower in the upper layers (0–20 cm) compared to deeper layers, where EFs can be up to five times higher. The most enriched elements based on average EF values are P (73.4), As (51.1), Pb (26.2), ^{238}U (25.8), and ^{226}Ra (22.9), all of which significantly exceed background levels. Other highly enriched elements include Cu (20.0), ^{230}Th

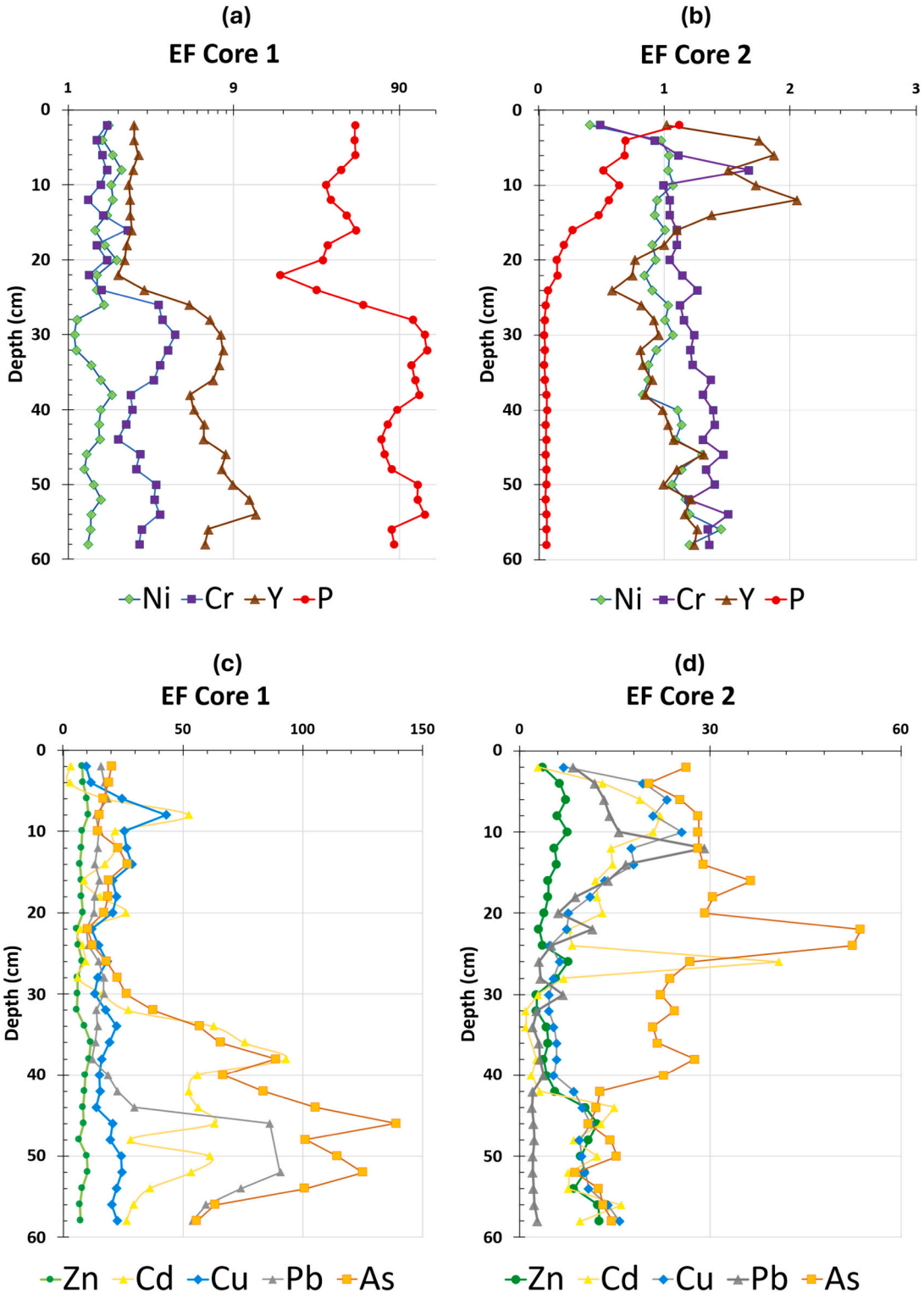

Fig. 5. Enrichment factor obtained for the trace elements and radionuclides in the case of the Core 1 and Core 2, where EF was calculated in relation to mean value of the core taken from Piedras estuary (see Table 1), considering Al as the normalizer element for the EF calculations.

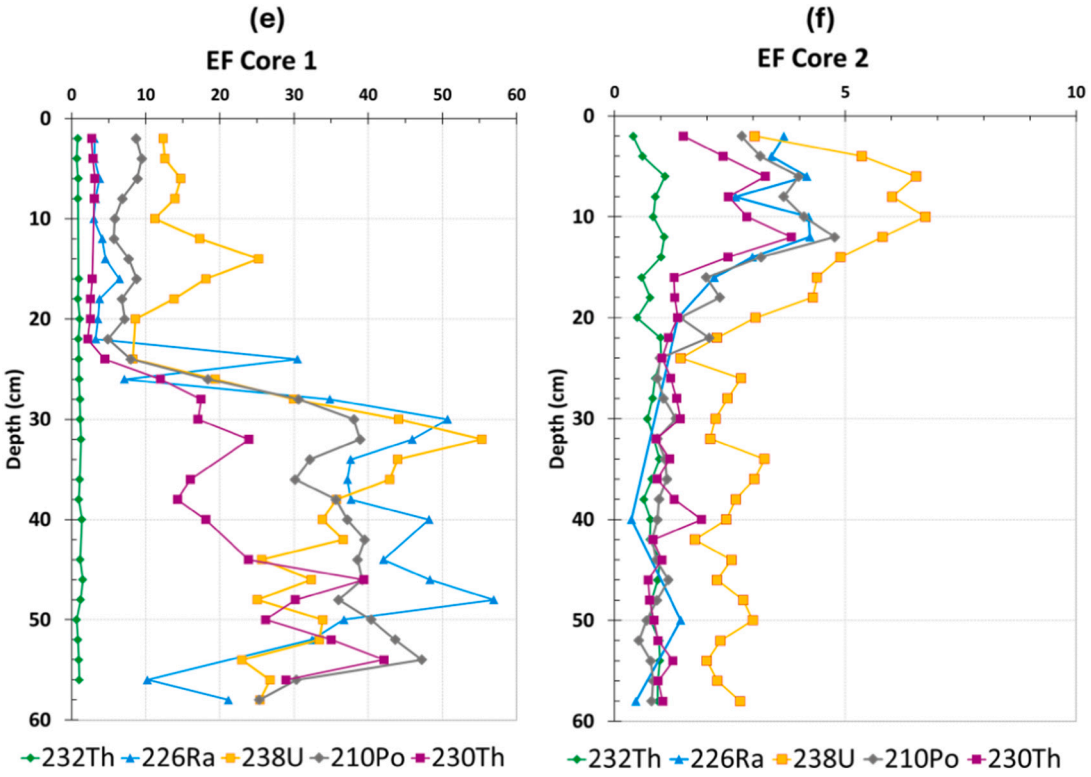

Fig. 5. (*continued*).

(16.1), and Fe (15.7), indicating a strong imprint of anthropogenic inputs.

Conversely, in Core 2, the average enrichment factors are generally lower throughout the sediment column, indicating a reduced influence from PG stacks. Significant evidence of anthropogenic enrichment does not appear until approximately 30 cm depth, which is consistent with the slower *sr* characteristic of this area of the estuary. On average, only a few elements, such as As with an EF of 23.9, Cd with 11.1, and Cu with 11.0, reach values classified as severe enrichment, while Pb and Zn, with values of 7.0 and 6.6 respectively, fall within the moderately severe category. The remaining elements show low to negligible average EF values, with P in particular exhibiting no enrichment (EF = 0.2).

The most pronounced disparity between the two cores is observed for P, whose enrichment factor in Core 1 is more than 300 times greater than in Core 2 confirming its strong association with PG discharges. Similarly, elements such as Ca, S, Mg, Cd, and ^{226}Ra display enrichment

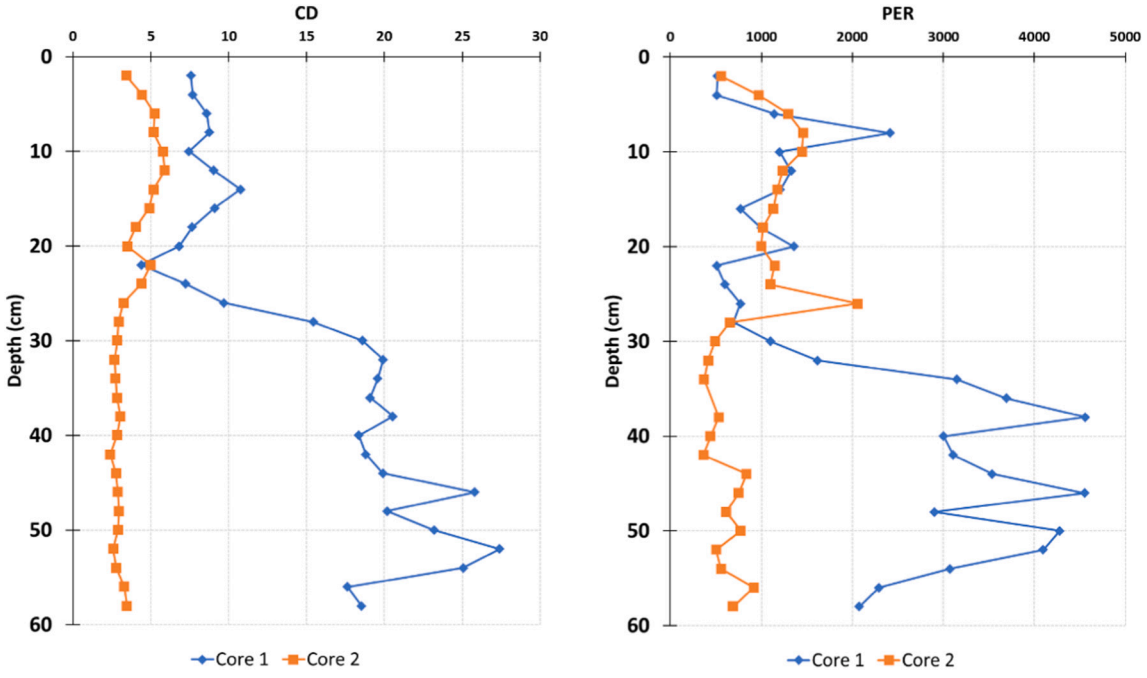

Fig. 6. Variation of the Contamination Degree (CD) and Potential Ecological Risk (PER) indices for the two sediment cores from the Tinto Estuary.

factors between 2 and 25 times higher in Core 1, reflecting their strong association with PG residues and their preferential accumulation near the discharge point. In contrast, the vertical profiles of Fe, Cr, Zn, and ^{210}Pb show comparable values in Core 2, suggesting that their distribution is primarily controlled by AMD or regional background contributions, rather than by localized industrial sources. This divergence in enrichment patterns highlights the dual impact of PG and AMD on the system.

The application of the Potential Ecological Risk Index (PER_i) and the Contamination Degree (CD) clearly highlights the contrast in contamination histories between the two sediment cores (Fig. 6).

In Core 1, PER_i values consistently exceed 600 throughout the entire profile, reaching peaks close to 4500 in the deeper layers, which corresponds to the period of open-cycle PG discharge. According to Hakanson's classification, these values indicate very severe ecological risk. Similarly, CD values increase progressively with depth, with an average value of 15.0, placing the core between the categories of "considerable" and "high contamination", and reflecting the stratified impact of industrial activity over time.

In contrast, Core 2 displays a much more attenuated signal. PERI values remain above 100, but only exceed 600 in the upper 30 cm, indicating that the contamination is mostly concentrated near the surface. Below this depth, values drop significantly, pointing to relatively uncontaminated sediments. The CD index supports this interpretation, remaining almost constant and below 6 between 30 and 60 cm—levels classified as low contamination. The average CD for Core 2 is 3.8, nearly four times lower than that of Core 1.

Altogether, these indices provide a coherent summary of the system's contamination history: while Core 1 preserves a clear vertical record of intense industrial inputs, Core 2 captures a more diffuse and surface-limited signal.

Finally, the Igeo index provides a clear comparison of contamination levels between the two cores (Fig. 7). Core 1 exhibits notably higher Igeo values for most elements, especially for P (Igeo = 5.6) and ^{238}U, Cd, Pb, Cu, and ^{226}Ra, which fall into the strong to very strong contamination categories. In contrast, Core 2 shows generally moderate to low Igeo values, with enrichment largely limited to As, Cd, Cu, Pb, and Zn, which are likely linked to diffuse contamination, regional background levels, or inputs from AMD. Notably, As shows similar values in both cores, suggesting a widespread and persistent source. Overall, the Igeo profiles are fully consistent with the vertical patterns described throughout this study, confirming that Core 1 records a stratified and intense contamination history associated with PG discharges, while Core 2 captures a more diffuse and diluted signal shaped by broader estuarine dynamics and lower sedimentation rates.

3.5. Correlations and statistics

To better understand the sources of contamination in the estuary, as well as the grouping and temporal evolution of elements, a principal component analysis (PCA) was performed on the sediment samples collected from Core 1 and Core 2 (see Fig. 8). Prior to conducting the PCA, normality tests were applied to the dataset, most variables did not follow a normal distribution.

In Core 1, the PCA reveals that F1 explains about 52 % of this variance. This factor displays high positive scores for elements such as P, As, Pb, Cd, Zn, S, and various radionuclides, all of which present elevated enrichment factors (EFs). These values indicate strong anthropogenic inputs, predominantly from PG residues and industrial discharges. On the negative side of F1, elements such as Al, Ni, Ti, and K, characterized by low or negligible EF values, are located, reflecting their predominantly natural origin. Factor 2, which explains 15.8 % of the variance, differentiates other elements (such as Cu, Zn, Cd, and radionuclides). It separates elements enriched by both industrial inputs and AMD on the positive side from those derived purely from direct PG contamination. Regarding the observation scores, most sediment samples plot on the positive side of F1 and correspond to deeper layers, associated with the period of direct waste discharge and thus higher contamination. In contrast, the more superficial layers show very low loadings on F1, indicating they are less impacted by residues from the stacks and suggesting a decline in contamination in more recent times.

In Core 2, the PCA shows that F1, explaining 45 % of this variance, groups on its positive side those elements typically enriched in the upper layers, linked to PG and all of which exhibit moderate to severe enrichment based on their enrichment factors (like P, radionuclides, Ca, S, As), whereas elements such as Fe and Zn appear on its negative side, possibly associated with deeper layers enriched by AMD. Meanwhile, F2 explains 24 % of the variance. In this case, certain elements (As, Fe) exhibit negative values, suggesting that this factor may capture an additional process or contamination source, likely stemming from the interaction of different inputs (fertilizer industry and AMD). Regarding the observation scores, the samples that plot closest to the elements directly associated with PG, particularly P and radionuclides, are found in the more superficial layers, where the recent influence of industrial activity is evident. In contrast, deeper layers tend to be associated with the elements on the negative side of F1 reflecting a stronger AMD signature in earlier stages.

4. Conclusions

This paper analyses the temporal evolution of pollution in the Tinto River Estuary (SW Spain), a system strongly impacted by both phosphogypsum (PG) stacks and acid mine drainage (AMD) discharges. To reconstruct the history and intensity of contamination, two sediment

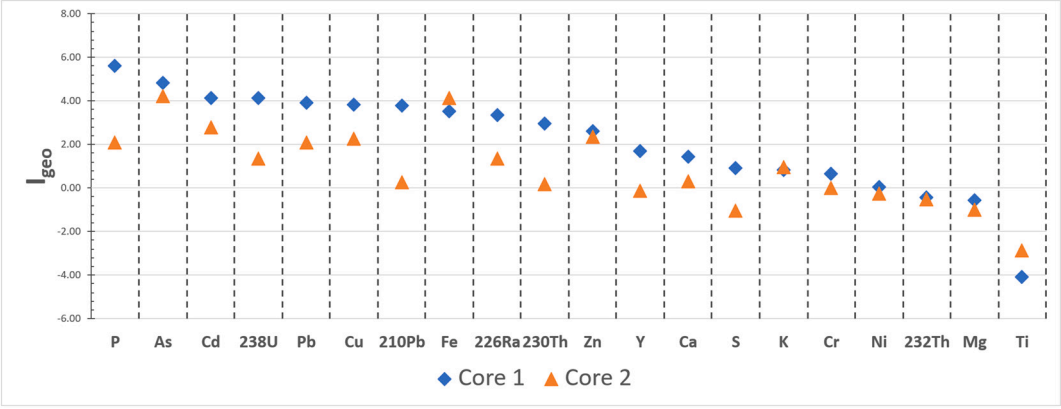

Fig. 7. Values of the I_{geo} average for the analyzed elements in the two sediment cores from the Tinto Estuary.

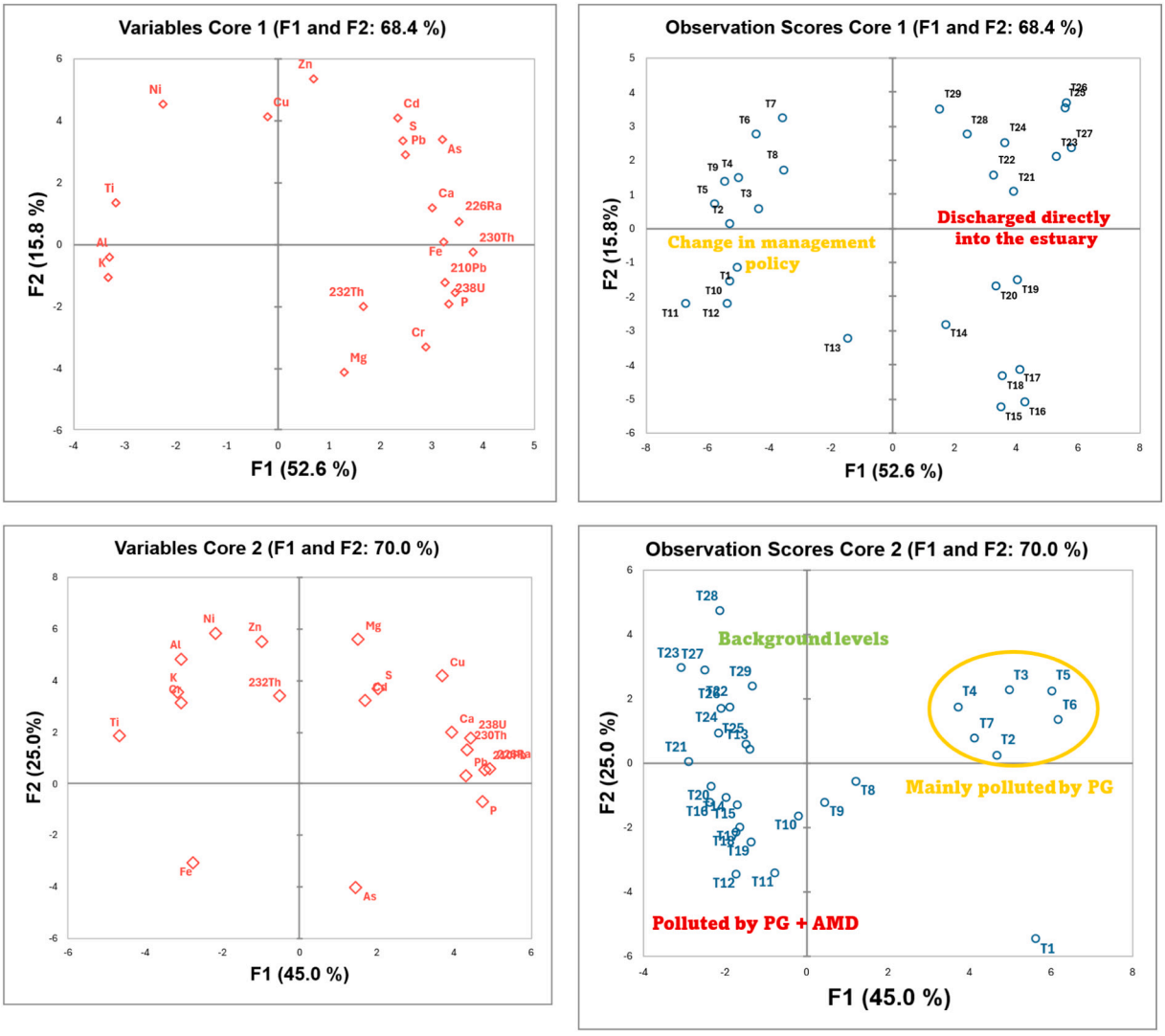

Fig. 8. Principal Component Analysis (PCA) displaying variable loadings and observation scores for Cores 1 and 2.

cores were studied from contrasting sites in the saltmarsh: one collected adjacent to the PG piles (Core 1) and the other from the opposite riverbank (Core 2). Concentrations of major and trace elements, heavy metals, and radionuclides from the ^{238}U series were determined and compared with background levels established from an uncontaminated reference site in the Piedras River estuary. The main conclusions obtained are as follows:

1. Core 1 records three distinct stages of industrial waste management in the Tinto estuary. The open-discharge stage (60–30 cm) is characterized by extreme enrichments, with P concentrations up to 4 %, ^{238}U reaching ~1200 Bq·kg^{-1}, ^{226}Ra ~800 Bq·kg^{-1}, As ~4700 μg·g^{-1}, and Pb ~3000 μg·g^{-1}, all exceeding ecotoxicological thresholds. The transition stage (30–10 cm) reflects decreasing concentrations of PG-associated elements, but persistent U and P inputs indicate continued leaching from PG piles. The recent stage (0–10 cm) shows marked reductions after the implementation of containment measures post-2010, with ^{238}U decreasing to ~400 Bq·kg^{-1}, ^{226}Ra to ~57 Bq·kg^{-1}, and P to ~1.5 %, though still above background levels.
2. Core 2, located on the opposite bank of the estuary, shows a more attenuated and temporally restricted contamination record. The influence of industrial activity is confined to the upper 20 cm, without clear evidence of the open-discharge stage. Radionuclides display much lower values than in Core 1, with ^{226}Ra up to ~80 Bq·kg^{-1} and ^{210}Pb ~90 Bq·kg^{-1}, while P reaches a maximum of ~1.5 % in surface sediments and declines to ~0.09 % at depth. Trace metals such as Fe, Cr, and Zn remain relatively stable, consistent with diffuse acid mine drainage (AMD) contributions rather than direct PG inputs.
3. Core 1 exhibits a sedimentation rate of ~1.2 cm/year, which provides high temporal resolution and allows for the clear identification of the three contamination phases. In contrast, Core 2 has a significantly lower sedimentation rate (~0.4 cm/year), which compresses the contamination record into a thinner sequence and likely limits its archival capacity.
4. Contamination indices in Core 1 (Igeo, CF, EF, PERI) reach their highest values during the open-discharge period, indicating extreme enrichment and very high ecological risk. In Core 2, these indices remain low and homogeneous, reflecting limited impact and a much lower ecological risk. The contrast between the two sites highlights the strong spatial asymmetry in contamination intensity and extent within the estuary.
5. Principal Component Analysis effectively separates natural background signals from PG-related contamination and AMD contributions. In Core 1, PG-related elements dominate the contamination signature, whereas in Core 2 the geochemical variability is mainly explained by AMD inputs combined with recent surface phosphorus enrichment.

6. Despite reductions in the upper layers of Core 1, current levels of U, ^{226}Ra, and P remain above background, evidencing the persistence of contamination driven by leaching from PG piles. In Core 2, the relatively stable and lower concentrations suggest reduced vulnerability, but the presence of AMD-derived elements highlights the need for continuous monitoring.

CRediT authorship contribution statement

M. del Caño-Mármol: Writing – original draft, Formal analysis, Data curation, Conceptualization. **A. Barba-Lobo:** Methodology, Investigation, Funding acquisition, Formal analysis, Data curation, Conceptualization, Supervision. **E.G. San Miguel:** Supervision, Resources, Methodology, Funding acquisition, Conceptualization. **J.L. Guerrero:** Methodology, Investigation, Formal analysis, Data curation. **J.P. Bolívar:** Supervision, Resources, Formal analysis, Conceptualization.

Declaration of competing interest

The authors declare that they have no known competing financial interests or personal relationships that could have appeared to influence the work reported in this paper.

Appendix A. Supplementary data

Supplementary data to this article can be found online at https://doi.org/10.1016/j.marpolbul.2025.118996.

Data availability

Data will be made available on request.

References

A. Valenzuela, T.D., Pascual, E., 2002. Secuencia de facien volcánicas en el área del río Odiel. Geoceta 32. https://sge.usal.es/archivos/geogacetas/Geo32/Art33.pdf.

Aduvire, O., 2006. Drenaje ácido de mina generación y tratamiento. Geológico y Minero de España Dirección de Recursos Minerales y Geoambiente, p. 140.

Barba-Lobo, A., Gázquez, M.J., Bolívar, J.P., 2022. A practical procedure to determine natural radionuclides in solid materials from mining. Minerals 12 (5), 5. https://doi.org/10.3390/min12050611.

Barba-Lobo, A., García-González, B., Guerrero, J.L., Bolívar, J.P., 2024. Sedimentary environmental quality of a biosphere reserve estuary in southwestern Iberian Peninsula. Mar. Pollut. Bull. 201, 116225. https://doi.org/10.1016/j.marpolbul.2024.116225.

Bolívar, J.P., García-Tenorio, R., García-León, M., 1995. Enhancement of natural radioactivity in soils and salt-marshes surrounding a non-nuclear industrial complex. Sci. Total Environ. 173-174, 125–136. https://doi.org/10.1016/0048-9697(95)04735-2.

Borrego, J., Morales, J., de la Torre, M., Grande, J., 2002. Geochemical characteristics of heavy metal pollution in surface sediments of the Tinto and Odiel river estuary (southwestern Spain). Environ. Geol. 41 (7), 785–796. https://doi.org/10.1007/s00254-001-0445-3.

Casanueva Marenco, M.J., 2014. Estudio analítico de la contaminación metálica en aguas afectadas por actividades antropogénicas crónicas. Métodos de control de la biodisponibilidad y toxicidad metálica. Universidad de Cadiz.

Chen, C.-W., Kao, C.-M., Chen, C.-F., Dong, C.-D., 2007. Distribution and accumulation of heavy metals in the sediments of Kaohsiung Harbor, Taiwan. Chemosphere 66 (8), 1431–1440. https://doi.org/10.1016/j.chemosphere.2006.09.030.

Chen, H., Chen, Z., Chen, Z., Ou, X., Chen, J., 2020. Calculation of toxicity coefficient of potential ecological risk assessment of rare earth elements. Bull. Environ. Contam. Toxicol. 104 (5), 582–587. https://doi.org/10.1007/s00128-020-02840-x.

Delgado, J., Boski, T., Nieto, J.M., Pereira, L., Moura, D., Gomes, A., Sousa, C., García-Tenorio, R., 2012. Sea-level rise and anthropogenic activities recorded in the late Pleistocene/Holocene sedimentary infill of the Guadiana Estuary (SW Iberia). Quat. Sci. Rev. 33, 121–141. https://doi.org/10.1016/j.quascirev.2011.12.002.

DelValls, T.A., Forja, J.M., Gonzalez-Mazo, E., Gomez-Parra, 1998. Determining contamination sources in marine sediments using multivariate analysis. Trends Anal. Chem. 17, 181–192. https://www.academia.edu/12564074/Determining_contamination_sources_in_marine_sediments_using_multivariate_analysis.

El Afifi, E.M., Hilal, M.A., Attallah, M.F., EL-Reefy, S.A., 2009. Characterization of phosphogypsum wastes associated with phosphoric acid and fertilizers production. J. Environ. Radioact. 100 (5), 407–412. https://doi.org/10.1016/j.jenvrad.2009.01.005.

Emmerson, R.H.C., O'Reilly-Wiese, S.B., Macleod, C.L., Lester, J.N., 1997. A multivariate assessment of metal distribution in inter-tidal sediments of the Blackwater Estuary, UK. Marine Pollution Bulletin 34 (11), 960–968. https://doi.org/10.1016/S0025-326X(97)00067-2.

Gao, M., Tang, J., Tu, Y., Zhu, M., Nie, Z., Liu, X., Liu, G., 2025. The response and ecological implications between various sulfur forms and environmental factors in acid mine drainage. Environ. Res. 275, 121425. https://doi.org/10.1016/j.envres.2025.121425.

Guerrero, J.L., Gutiérrez-Álvarez, I., Mosqueda, F., Olías, M., García-Tenorio, R., Bolívar, J.P., 2019. Pollution evaluation on the salt-marshes under the phosphogypsum stacks of Huelva due to deep leachates. Chemosphere 230, 219–229. https://doi.org/10.1016/j.chemosphere.2019.04.212.

Hakanson, L., 1980. An ecological risk index for aquatic pollution control.a sedimentological approach. Water Res. 14 (8), 975–1001. https://doi.org/10.1016/0043-1354(80)90143-8.

Hierro, A., Martín, J.E., Olías, M., Vaca, F., Bolivar, J.P., 2013. Uranium behaviour in an estuary polluted by mining and industrial effluents: the Ría of Huelva (SW of Spain). Water Res. 47 (16), 6269–6279. https://doi.org/10.1016/j.watres.2013.07.044.

Hossain, M.B., Marshall, D.J., Venkatramanan, S., 2014. Sediment granulometry and organic matter content in the intertidal zone of the Sungai Brunei estuarine system, northwest coast of Borneo, 9 (2), 231–239.

Kerolli–Mustafa, M., Fajković, H., Rončević, S., Ćurković, L., 2015. Assessment of metal risks from different depths of jarosite tailing waste of Trepça Zinc Industry, Kosovo based on BCR procedure. J. Geochem. Explor. 148, 161–168. https://doi.org/10.1016/j.gexplo.2014.09.001.

Liu, J., Peng, A., Deng, S., Liu, M., Liu, G., Li, C., 2021. Distribution of heavy metals and radionuclides in the sediments and their environmental impacts in Nansha Sea area, South China Sea. Mar. Pollut. Bull. 166, 112192. https://doi.org/10.1016/j.marpolbul.2021.112192.

Macías, F., Cánovas, C.R., Cruz-Hernández, P., Carrero, S., Asta, M.P., Nieto, J.M., Pérez-López, R., 2017. An anomalous metal-rich phosphogypsum: characterization and classification according to international regulations. J. Hazard. Mater. 331, 99–108. https://doi.org/10.1016/j.jhazmat.2017.02.015.

Mas, J.L., San Miguel, E.G., Bolívar, J.P., Vaca, F., Pérez-Moreno, J.P., 2006. An assay on the effect of preliminary restoration tasks applied to a large TENORM wastes disposal in the south-west of Spain. Sci. Total Environ. 364 (1), 55–66. https://doi.org/10.1016/j.scitotenv.2005.11.006.

Müller, G., 1979. Index of geoaccumulation in sediments of the Rhine River. J. Geol. 2 (3), 108–118.

Nieto, J.M., Sarmiento, A.M., Olías, M., Canovas, C.R., Riba, I., Kalman, J., Delvalls, T.A., 2007. Acid mine drainage pollution in the Tinto and Odiel rivers (Iberian Pyrite Belt, SW Spain) and bioavailability of the transported metals to the Huelva Estuary. Environ. Int. 33 (4), 445–455. https://doi.org/10.1016/j.envint.2006.11.010.

Olías, M., Cánovas, C.R., Nieto, J.M., Sarmiento, A.M., 2006. Evaluation of the dissolved contaminant load transported by the Tinto and Odiel rivers (South West Spain). Appl. Geochem. 21 (10), 1733–1749. https://doi.org/10.1016/j.apgeochem.2006.05.009.

Papaslioti, E.-M., Giampouras, M., Sánchez-López, L., Basallote, M.D., Freydier, R., Cánovas, C.R., Pérez-López, R., 2024. Temporal dynamics of contaminants in an estuarine system affected by acid mine drainage discharges. Sci. Total Environ. 947, 174683. https://doi.org/10.1016/j.scitotenv.2024.174683.

Pérez-López, R., Macías, F., Cánovas, C.R., Sarmiento, A.M., Pérez-Moreno, S.M., 2016. Pollutant flows from a phosphogypsum disposal area to an estuarine environment: an insight from geochemical signatures. Sci. Total Environ. 553, 42–51. https://doi.org/10.1016/j.scitotenv.2016.02.070.

Pérez-López, R., Cánovas, C.R., Macías, F., Basallote, M.D., Freydier, R., Olías, M., Nieto, J.M., 2025. Tracing acid mine drainage from an accidental spill on the Estuary of Huelva (SW Spain). Environ. Pollut. 372, 126033. https://doi.org/10.1016/j.envpol.2025.126033.

Qingjie, G., Jun, D., Yunchuan, X., Qingfei, W., Liqiang, Y., 2008. Calculating pollution indices by heavy metals in ecological geochemistry assessment and a case study in parks of Beijing. J. China Univ. Geosci. 19 (3), 230–241. https://doi.org/10.1016/S1002-0705(08)60042-4.

Restore 20/30 – Proyecto de clausura de las balsas de fosfoyeso. (s. f.), May 16th, 2025. Recuperado 16 de mayo de 2025 de. https://restore2030.com/.

Rudnick, R.L., Gao, S., 2003. 3.01—composition of the continental crust. In: Holland, H. D., Turekian, K.K. (Eds.), Treatise on Geochemistry. Pergamon, pp. 1–64. https://doi.org/10.1016/B0-08-043751-6/03016-4.

Sáez, R., Pascual, E., Toscano, M., Almodóvar, G.R., 1999. The Iberian type of volcano-sedimentary massive sulphide deposits. Miner. Deposita 34 (5), 549–570. https://doi.org/10.1007/s001260050220.

Sainz, A., Grande, J.A., De La Torre, M.L., 2004. Characterisation of heavy metal discharge into the Ria of Huelva. Environ. Int. 30 (4), 557–566. https://doi.org/10.1016/j.envint.2003.10.013.

Sousa, C.A.M., Delgado, J., Szalaj, D., Boski, T., 2019. Holocene background concentrations and actual enrichment factors of metals in sediments from Ria Formosa, Portugal. Marine Pollution Bulletin 149, 110533. https://doi.org/10.1016/j.marpolbul.2019.110533.

Tripathi, D.P., Nema, A.K., 2025. Evaluation of ecological risk due to suspended particulate matter-bound heavy metals deposited on selected plants in an urban area. Urban Clim. 59, 102293. https://doi.org/10.1016/j.uclim.2025.102293.

van Geen, A., Adkins, J.F., Boyle, E.A., Nelson, C.H., Palanques, A., 1997. A 120-yr record of widespread contamination from mining of the Iberian pyrite belt. Geology 25 (4), 291–294. https://doi.org/10.1130/0091-7613(1997)025<0291:AYROWC>2.3.CO;2.

Vidal-Garduño, R., Terrones-Saeta, J.M., Suárez-Macías, J., Macías, E.M.R., 2025. Mining dams as industrial and environmental heritage: the mining dams of Huelva (Spain). Geoheritage 17 (2), 80. https://doi.org/10.1007/s12371-025-01125-1.

Wang, W., Wang, W.-X., 2016. Phase partitioning of trace metals in a contaminated estuary influenced by industrial effluent discharge. Environ. Pollut. 214, 35–44. https://doi.org/10.1016/j.envpol.2016.03.059.

Williams, N., Block, K.A., 2015. Spatial and vertical distribution of metals in sediment cores from Río Espíritu Santo estuary, Puerto Rico, United States. Marine Pollution Bulletin 100 (1), 445–452. https://doi.org/10.1016/j.marpolbul.2015.08.007.